Journal of the Serbian Chemical Society
JSCS-info@shd.org.rs • www.shd.org.rs/JSCS
J. Serb. Chem. Soc. *86* (11) 1103–1112 (2021)
JSCS–5486
Original scientific paper
Published 24 September 2021

Hydroxyapatite/nifuroxazide conjugate: Characterization, drug release and antimicrobial activity

ŽELJKO RADOVANOVIĆ[1]*, KATARINA MIHAJLOVSKI[2], LIDIJA RADOVANOVIĆ[1#], ĐORĐE JANAĆKOVIĆ[2] and RADA PETROVIĆ[2]

[1]*Innovation Centre of the Faculty of Technology and Metallurgy, University of Belgrade, Karnegijeva 4, 11000 Belgrade, Serbia and* [2]*Faculty of Technology and Metallurgy, University of Belgrade, Karnegijeva 4, 11000 Belgrade, Serbia*

(Received 20 April, revised 25 May, accepted 26 May 2021)

Abstract: Synthetic hydroxyapatite ($Ca_{10}(PO_4)_6(OH)_2$, HAp) is very similar to the inorganic part of the bones and teeth of mammals. It is a well-known biomaterial with good biocompatibility, osteoconductivity and bioactivity. Nifuroxazide ($C_{12}H_9N_3O_5$, NFX) is a broad-spectrum antibacterial drug and poorly soluble in water. In order to increase the solubility of NFX, nano-sized HAp powder and raw NFX drug were mixed giving, as a result, a HAp/NFX conjugate. Characterization of the raw materials and the obtained conjugate confirmed the integration of NFX on the HAp surface. An *in vitro* study of drug release in simulated stomach acid and intestinal fluid showed a much faster release of NFX from HAp surface than those of the raw drug. The HAp/NFX conjugate showed excellent inhibitory effects against Gram-positive bacterium *Staphylococcus aureus*, Gram-negative bacterium *Escherichia coli* and yeast *Candida albicans*, proving the nano-sized HAp powder as a promising drug carrier.

Keywords: biomaterials; nanomaterials; drug delivery; antimicrobial properties.

INTRODUCTION

Hydroxyapatite ($Ca_{10}(PO_4)_6(OH)_2$, HAp) as a nano-sized and calcium-deficient material is the main inorganic component of the bones and teeth of mammals.[1] Due to its excellent bioactivity, biocompatibility, osteoconduction and osteoinduction, the broad spectrum of applications of HAp is known so far: in bone tissue engineering, implant osteointegration[1] together with being a gene, protein and drug carrier.[2–6] Drug carriers based on HAp have been of particular

* Corresponding author. E-mail: zradovanovic@tmf.bg.ac.rs
# Serbian Chemical Society member.
https://doi.org/10.2298/JSC210420040R

interest during the last decades, especially for the promising treatment of bone infections, arthritis, cancer and cardiovascular diseases.[7–9]

Nifuroxazide ($C_{12}H_9N_3O_5$, NFX), a poorly water-soluble drug that belongs to the class of nitrofuran derivatives, shows significant antibacterial activity against Gram-positive bacteria, such as *Staphylococcus aureus* and *Streptococcus spp*., and Gram-negative bacteria, such as *Escherichia coli* and *Pseudomonas aeruginosa*. Due to the presence of a nitro group in its structure, NFX is efficient in the treatment of infections in the gastrointestinal and urogenital tracts, and is known to have a bacteriostatic effect in small doses as well as a bactericidal effect in high doses.[10] Furthermore, there are studies that proved NFX as a promising drug in the treatment of different types of cancer.[10–12] Nevertheless, NFX, which was frequently used for treatment of colitis and diarrhoea, showed low effect against those diseases due to poor absorption from the digestive tract (low burst effect) that resulted in fast removal from the body without being metabolized.[13] Some studies showed that improvement of the efficiency (faster dissolution rate and higher solubility) of low soluble drugs such as carvedilol, ibuprofen and silybin, can be achieved by integration with HAp.[5,6,14] It is assumed that the connection between HAp and drugs occurred mainly through establishment of hydrogen bonds between OH groups at the HAp surface and some of the functional groups of the drug.[5,6]

In the current study, HAp nanoparticles were prepared by the hydrothermal method, while HAp/NFX conjugate was obtained by impregnation under vacuum. The structure, morphology, specific surface area, spectral and thermal properties of HAp, raw NFX and HAp/NFX conjugate were investigated by X-ray powder diffraction (XRPD), Field emission scanning electron microscopy (FESEM), the Brunauer, Emmett and Teller method (BET), attenuated total reflectance-Fourier transform infrared spectroscopy (ATR-FTIR) and thermal analysis. *In vitro* drug release tests in simulated gastric and intestinal fluids were performed for NFX and HAp/NFX, while all materials were studied *in vitro* for their antimicrobial activities.

EXPERIMENTAL

Materials and measurements

For the synthesis of HAp powder, calcium nitrate tetrahydrate (≥ 98 %, Carl Roth, Germany), sodium dihydrogen phosphate dihydrate (99.8 %, VWR), and ammonium hydroxide (*p.a.,* Zorka Pharma, Šabac, Serbia) were used. Nifuroxazide (5-nitro-2-furaldehyde *p*-hydroxybenzoylhydrazone) was purchased from Sigma–Aldrich.

XRPD measurements were performed on a Rigaku SmartLab diffractometer using CuKα radiation, at 40 kV and 30 mA, in Bragg–Brentano geometry. Diffraction data for HAp and HAP/NFX were collected in the range $5° < 2\theta < 70°$ (scan speed: 0.12° min^{-1}, step width: $2\theta = 0.01°$), whereas diffraction data for NIF were collected in the range $5° < 2\theta < 50°$ (scan speed: 0.06° min^{-1}, step width: $2\theta = 0.01°$) at room temperature. ATR-FTIR spectra of the samples were recorded in absorbance mode using a Nicolet™ iS™ 10 FTIR spectrometer

(Thermo Fisher Scientific) with Smart iTR™ ATR sampling accessories, within the range of 4000–400 cm^{-1}, at a resolution of 4 cm^{-1} and in 20 scan mode. Thermal properties were examined from room temperature up to 1200 °C for HAp and HAp/NFX and up to 800 °C for NFX in platinum sample cups using an SDT Q600 instrument (TA Instruments). The heating rate was 20 °C min^{-1} and the furnace atmosphere consisted of air at a flow rate of 100 mL min^{-1} (weight accuracy is ±1 %). FESEM Tescan Mira 3 XMU was used for the morphological characterization of the samples. Before analysis, the samples were coated with Au. The specific surface areas (*SSA*) of HAp, NFX and HAp/NFX were calculated according to the Brunauer, Emmett and Teller (BET) method from the linear part of the nitrogen adsorption isotherm at 77 K on a Micrometrics ASAP 2020 instrument. Before the measurements, the samples were out-gassed at 150 °C for 10 h under vacuum. The total pore volume (V_{tot}) was given at p/p_0 = 0.998. The volume of the mesopores was calculated according to the Barrett, Joyner and Halenda (BJH) method from the desorption branch of the isotherm.

Synthesis of nano-sized HAp and HAp/NFX conjugate

Nano-HAp was obtained as reported earlier.[15] Briefly, appropriate amounts of $Ca(NO_3)_2 \cdot 4H_2O$, $NaH_2PO_4 \cdot 2H_2O$ and NH_4OH were dissolved in 2 L of distilled water. The obtained solution with Ca/P ratio 1.67 and pH 10.10 was placed in an autoclave for 3 h at 160 °C. After slow cooling, the obtained powder was filtered and dried.

The HAp/NFX conjugate was prepared according to the following procedure: commercial drug NFX (0.14 g) was dissolved in 1 M NaOH (5 mL) under vigorous magnetic stirring. Next, HAp (0.60 g) was added to the solution and stirred for 30 min. The obtained mixture was transferred into round bottom flask (100 mL) and stirred in a rotavapor at 60 °C for 45 min until most of the solvent has evaporated. Then, the prepared sample was dried in an oven at 100 °C for 1 h and spontaneously cooled to the room temperature.

In vitro *drug release study*

In vitro drug release tests for NFX and HAp/NFX were performed in two types of fluids: aqueous solution of HCl (pH 1.2) and phosphate buffer solution (pH 6.8), which simulated stomach acid and intestinal fluid, respectively. 450 mL of each fluid was used for analysis, at 37 °C under continuous stirring rate of 100 rpm. Then 1 mg of NFX as well as 5.28 mg of HAP/NFX, containing 1 mg of NFX, was added to each fluid. At predetermined time intervals, an aliquot of 2.5 mL was taken for analysis and 2.5 mL of fresh fluid was added immediately, to maintain a constant volume. The aliquot was filtered and then analysed by UV–Vis spectrophotometry (UV-1800, Shimadzu, Japan) at a wavelength of 255 nm. The reported results were an average value of two measurements.

Antimicrobial test

Quantitative tests of the antimicrobial activity of HAp, NFX and HAp/NFX samples against Gram-positive (G^+) bacterium *Staphylococcus aureus* (*S. aureus*, ATCC 25923), Gram-negative (G^-) bacterium *Escherichia coli* (*E. coli*, ATCC 25922) and yeast *Candida albicans* (*C. albicans*, ATCC 10259) were performed according to the liquid challenge method in sterile normal saline solution. A mass of 0.01 g of each sample was suspended in a tube containing 0.9 mL of sterile normal saline and inoculated with 0.9 mL microorganism suspension to achieve the appropriate concentrations (in CFU cm^{-1}). The tubes were then incubated at 37 °C for 1 h. After incubation, 9 mL of sterile normal saline was added. Subsequently, 1 mL aliquots were taken as samples for determination of the viable cell. Sterile normal saline solution was used for dilution of the number of colonies and 0.1 mL of the appropriately diluted solution was placed in a Petri dish and overlaid with TSAY (Tripton soy

agar with 0.6 % yeast extract). The Petri dishes were incubated at 37 °C for 24 h. As a control, a blank sterile normal saline solution without sample was used. The degree of reduction, R / %, was calculated according to Eq. (1):

$$R = 100(CFU_{cont} - CFU_M)/CFU_{cont} \quad (1)$$

where CFU_{cont} is the number of microorganism colonies in the control tube and CFU_M is the number of microorganism colonies in the tubes with the samples.

RESULTS AND DISCUSSION

The XRPD patterns of HAp nanoparticles, NFX, and the HAp/NFX conjugate are shown in Fig. 1. The details about the crystal structure and Rietveld refinement analysis of the prepared nanosized HAp can be found in a previous study.[15] As could be observed from the patterns, HAp and NFX are highly crystalline, whereas HAp/NFX conjugate does not show the reflections characteristic for NFX but shows only broad reflections of a HAp phase, probably due to formation of highly dispersed and/or amorphous thin layer of NFX, which was similarly found in previous studies for other drugs.[5,6]

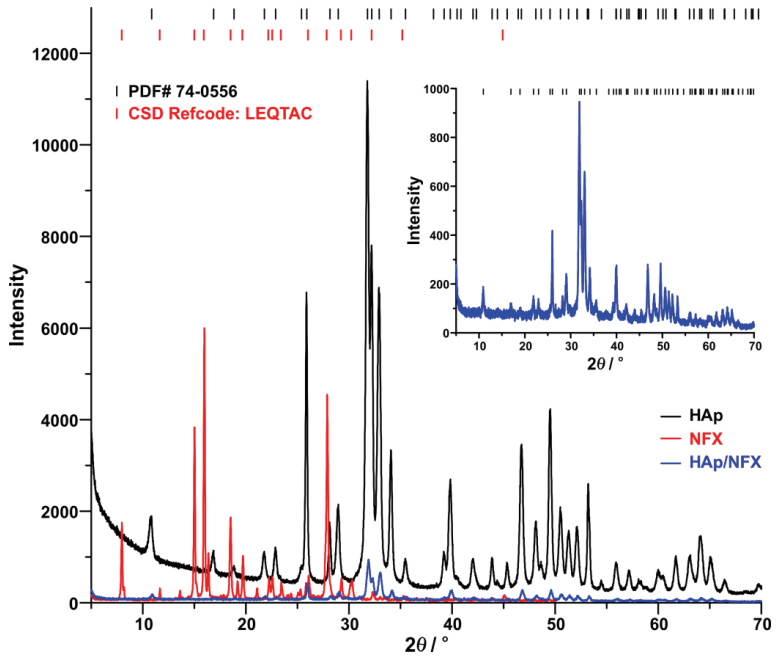

Fig. 1. XRPD patterns of HAp, NFX and HAp/NFX. The XRPD pattern of HAp is compared with the standard PDF# 74-0556 card. The XRPD pattern of NFX is compared with the pattern obtained from single crystal data (Cambridge Structural Database, CSD Refcode: LEQTAC).[16] An enlarged diffractogram of HAp/NFX is shown as the inset.

The FTIR spectra of HAp, NFX and HAP/NFX are presented in Fig. 2a. The characteristic bands corresponding to the presence of the OH^- and PO_4^{3-} groups

on the surface of the HAp are found at 3572 cm^{-1} as well as at 1088, 1020 and 560 cm^{-1}. These groups can, according to Zhao *et al.*,[5] improve the water solubility of insoluble drugs. In the spectrum of NFX, the band found at 1254 cm^{-1} can be assigned to the deformation of the furan ring, while the bands observed at 1465 and 851 cm^{-1} correspond to ν(C–C) and ν(C–H) vibrations of the phenyl ring, respectively. The presence of the N–H and C=O bonds is confirmed by the band at 3363 cm^{-1} for the former and at 1667 cm^{-1} for the later, while the vibration at 1606 cm^{-1} is ascribed to the C=N bond. In addition, the asymmetric (ν_{as}) and symmetric (ν_s) vibrations at 1507 and 1360 cm^{-1}, respectively, are ascribed to the existence of the resonant NO_2 group.[17] In the FTIR spectrum of HAp/NFX the characteristic group of bands of NFX, which are observed in the 1700–1200 cm^{-1} region, are slightly shifted towards lower wavelengths relative to the position of the same bands in the spectrum of raw NFX. In addition, the broad band centred at 3220 cm^{-1} indicates that there could be the connection of NFX with the HAp surface, probably through the formation of hydrogen bonds between NO_2 or C=O groups from NFX and OH^- group from HAp.[18]

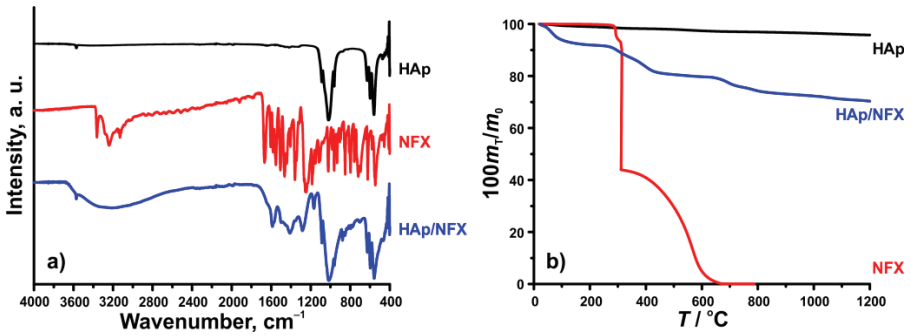

Fig. 2. FTIR spectra (a) and TGA curves (b) of HAp, NFX and HAp/NFX.

In order to determine the amount of drug in HAp/NFX,[5] the TGA analysis was performed in an air atmosphere and the results are presented in Fig. 2b. The TGA curve for HAp revealed a negligible mass loss of 4.3 %. In the temperature range investigated, the TGA curve of NFX shows stability up to ≈280 °C after which the combustion reaction of NFX occurs rapidly with a total mass loss of 100 % up to ≈650 °C. In the TGA curve of HAp/NFX, the observed mass loss of 6.1 % up to 100 °C was ascribed to the loss of adsorbed moisture, whereas the total mass loss up to final temperature of the analysis was 29.8 %.[19] According to the obtained data, it was found that the prepared HAp/NFX had a drug loading efficiency up to 19.4 %, which is close to theoretical value of 18.9 %. The difference between found and theoretical value of drug loading is in accordance with the weight accuracy of the instrument.

The FESEM micrographs of HAp, NFX and the HAp/NFX conjugate are presented in Fig. 3. As it has been shown earlier,[15] HAp consists of rod-like nanoparticles with an average size of 87 nm, which further form the agglomerates with sizes in the range 2–5 μm. The NFX drug is comprised of plate-like particles with wide particle size distributions (length in the range 0.3–10 μm, and width in the range 0.1–8 μm). The analysis of morphology of HAp/NFX shows that particles of HAp were overlaid by drug, with a thicker coating of the drug in some segments. The damage of the sample caused by the electron beam was not detected, which indicates that a thin layer of drug was formed on the surface of HAp.[6] In addition, the agglomeration of HAp/NFX conjugate is more pronounced than those of raw HAp and NFX, and HAP/NFX agglomerates are more compact.

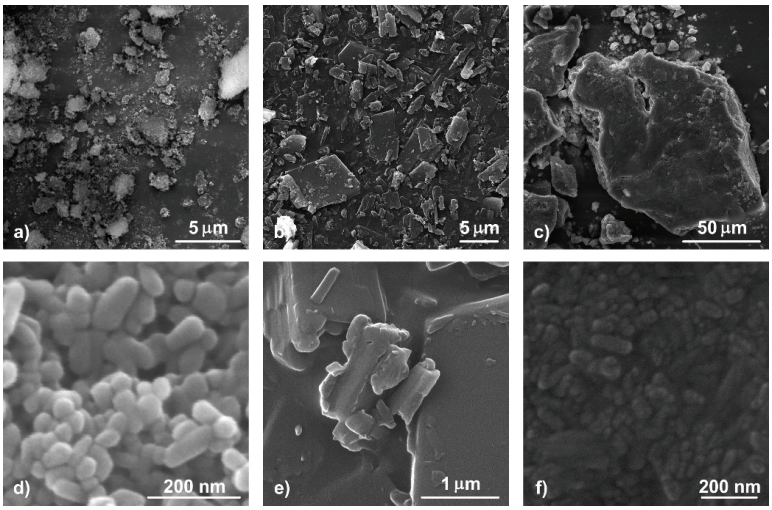

Fig. 3. FESEM images of HAp (a), NFX (b), HAp/NFX (c), HAp (d), NFX, (e) and HAp/NFX (f).

The morphology analysis of the samples is in accordance with the results of the BET analysis (Fig. 4, Table I). The value of *SSA* for the HAp/NFX conjugate was significantly smaller (0.24 m^2 g^{-1}) in comparison to values for HAp and NFX (47.8 and 3.51 m^2 g^{-1}, respectively), indicating a very good integration of the starting materials into HAp/NFX. The pores present in HAp sizes 20–30 nm were due to the voids between the nanoparticles. During the formation of a homogeneous mixture of HAp and NFX, these pores closed quite easily resulting in a low total porosity of the HAp/NFX conjugate.

The cumulative release profiles of raw NFX and NFX from the HAp/NFX conjugate in simulated stomach acid (pH 1.2) and intestinal fluid (pH 6.8) are shown in Fig. 5.

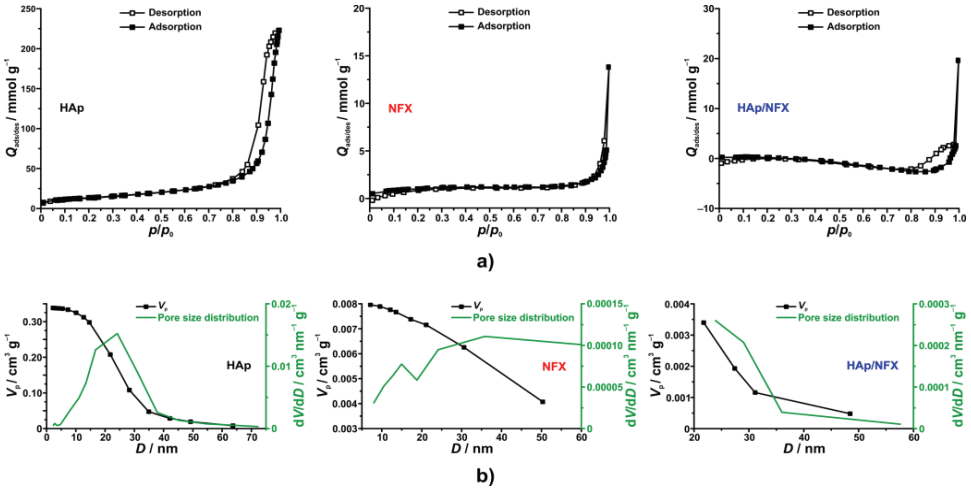

Fig. 4. Adsorption-desorption curves (a) and pore volume and pore size distribution (b) for HAp, NFX and HAp/NFX.

TABLE I. The results of BET analysis of HAp, NFX and HAp/NFX

Sample	*SSA* / m^2 g^{-1}	V_{tot}[a] / mL g^{-1}	V_{meso}[b] / mL g^{-1}	V_{micro}[c] / mL g^{-1}	D_{sr}[d] / nm	D_{max}[e] / nm
HAp	47.8	0.3395	0.3384	0.0142	20.2	24
NFX	3.51	0.0094	0.0080	0.0013	35.1	36
HAp/NFX	0.24	0.0044	0.0034	0.0007	29.5	–[f]

[a]V_{tot} – total pore volume; [b]V_{meso} – mesopore volume; [c]V_{micro} – micropore volume; [d]D_{sr} – average pore diameter; [e]D_{max} – the diameter of the pores that occupy the largest part of the volume. [f]Due to the low value of *SSA*, there was not enough data to determine D_{max} and there are negative values on the adsorption-desorption curves (Fig. 4)

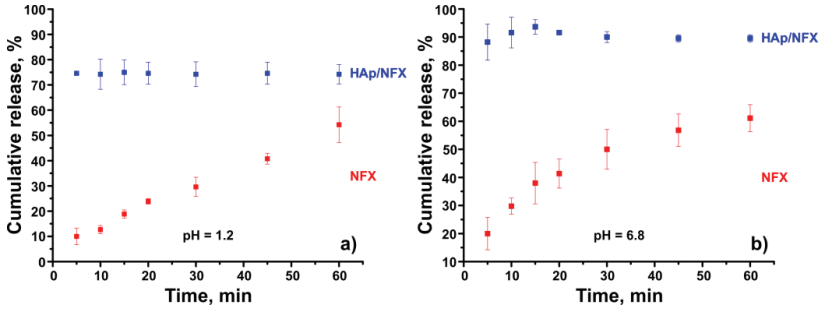

Fig. 5. *In vitro* drug release profiles of NFX and HAp/NFX at pH 1.2 (a) and 6.8 (b).

The release profile of raw NFX exhibited a slow, constant increase with time in both simulated fluids. After 60 min, 54 % of raw NFX in the stomach acid and 61 % in intestinal fluid had been excreted. Nevertheless, the HAp/NFX conjugate showed an initial fast release of NFX (burst effect) in both fluids, which could be associated with the integration of the drug with the surface of HAp.[20] A very high cumulative release of NFX from HAp/NFX was observed in the simulated

intestinal fluid with the value of 90 %. Such a releasing profile is more favourable from the point of its application proving that a combination of NFX with HAp leads to significantly better and faster utilization of the drug.

The *in vitro* antimicrobial activities of HAp, NFX and HAp/NFX were screened against *S. aureus* (as a G^+ bacterium), *E. coli* (as a G^- bacterium) and yeast *C. albicans* and the obtained results are presented in Table II. The HAp/NFX conjugate was found to be the most active, showing a high inhibitory effect against all examined bacteria (99.0 % for *S. aureus* and 94.0 % for *E. coli*) and moderate activity against *C. albicans* (Table II). In contrast to HAp/NFX, pure HAp and pure NFX were less effective, with the latter showing a high activity only against *S. aureus* (94.3 %). Such results are in agreement with the NFX release from HAp/NFX conjugate. Furthermore, it must be taken into account that excellent antimicrobial activity of HAp/NFX is achieved with about five times smaller mass of drug than that of pure NFX, which makes these results even more convincing.

TABLE II. The data of the antimicrobial test of HAp, NFX and HAp/NFX

Sample	*S. aureus*		*E. coli*		*C. albicans*	
	Number of colonies	$R \pm SD$ / %	Number of colonies	$R \pm SD$ / %	Number of colonies	$R \pm SD$ / %
Control	4.0×10^5	–	1.0×10^5	–	1.9×10^7	–
HAp	5.8×10^5	n. a.[a]	2.7×10^5	n. a.	8.0×10^6	57.9±1.4
NFX	2.3×10^4	94.3±1.1	5.2×10^4	48.0±1.7	7.9×10^6	58.4±0.6
HAp/NFX	4.0×10^3	99.0±0.7	6.0×10^3	94.0±1.2	7.1×10^6	62.6±1.0

[a]Not active

CONCLUSIONS

The low crystalline HAp/NFX conjugate was prepared successfully by impregnation of nanosized HAp with NFX under vacuum. The FTIR analysis showed the presence of hydrogen bonding between NFX and HAp, while the TGA analysis revealed a maximum drug loading efficiency. The *in vitro* release tests showed that HAp nanoparticles demonstrated immediate burst effect during NFX release, compared to that of raw NFX in simulated gastric and intestinal fluid. According to the *in vitro* antimicrobial study, the HAp/NFX conjugate showed the highest inhibitory activity, reaching more than 94 % inhibition against *S. aureus* and *E. coli*. The results of this study demonstrate that nanosized HAp is a suitable carrier for a poorly water-soluble drug. This could improve the release rate as well as antibacterial and antifungal activity of the drug.

Acknowledgement. This work was supported by the Ministry of Education, Science and Technological Development of the Republic of Serbia (Contract No. 451-03-68/2021-14/ /200287 and Contract No. 451-03-68/2021-14/200135).

ИЗВОД

ХИДРОКСИАПАТИТ/НИФУРОКСАЗИД КОЊУГАТ: КАРАКТЕРИЗАЦИЈА, ОТПУШТАЊЕ ЛЕКА И АНТИМИКРОБНА АКТИВНОСТ

ЖЕЉКО РАДОВАНОВИЋ[1], КАТАРИНА МИХАЈЛОВСКИ[2], ЛИДИЈА РАДОВАНОВИЋ[1], ЂОРЂЕ ЈАНАЋКОВИЋ[2] и РАДА ПЕТРОВИЋ[2]

[1]Иновациони центар Технолошко–металуршког факултета, Универзитет у Београду, Карнегијева 4, 11000 Београд и [2]Технолошко–металуршки факултет, Универзитет у Београду, Карнегијева 4, 11000 Београд

Синтетисани хидроксиапатит ($Ca_{10}(PO_4)_6(OH)_2$, HAp) веома је сличан неорганском делу кости и зуба сисара. То је познат биоматеријал са добром биокомпатибилношћу, остеокондуктивношћу и биоактивношћу. Нифуроксазид ($C_{12}H_9N_3O_5$, NFX) је антибиотски лек широког спектра и слабо растворан у води. Како би се повећала растворљивост лека NFX, припремљен је HAp/NFX коњугат мешањем HAp наночестичног праха и лека NFX. Карактеризацијом почетних материјала и добијеног коњугата потврђено је повезивање лека са површином HAp праха. Испитивање отпуштања лека *in vitro* у симулираној стомачној киселини и симулираној цревној течности показало је знатно брже отпуштање NFX са површине HAp у односу на отпуштање чистога лека. HAp/NFX коњугат показао је одличан инхибиторски ефекат на Грам-позитивну бактерију *Staphylococcus aureus*, Грам-негативну бактерију *Escherichia coli* и гљивицу *Candida albicans*, чиме је доказано да је наночестични HAp обећавајући носач лека.

(Примљено 20. априла, ревидирано 25. маја, прихваћено 26.маја 2021)

REFERENCES

1. S. V. Dorozhkin, *Hydroxyapatite and Other Calcium Orthophosphates*, Nova Publisher, New York, 2017 (ISBN: 978-1-53611-897-1)
2. J. Klesing, S. Chernousova, M. Epple, *J. Mater. Chem.* **22** (2012) 199 (https://dx.doi.org/10.1039/C1JM13502C)
3. T. Matsumoto, M. Okazaki, M. Inoue, S. Yamaguchi, T. Kusunose, T. Toyonaga, Y. Hamada, J. Takahashi, *Biomaterials* **25** (2004) 3807 (https://dx.doi.org/10.1016/j.biomaterials.2003.10.081)
4. T. S. P. Cellet, G. M. Pereira, E. C. Muniz, R. Silva, A. F. Rubira, *J. Mater. Chem., B* **3** (2015) 6837 (https://dx.doi.org/10.1039/c5tb00856e)
5. Q. Zhao, T. Wang, J. Wang, L. Zheng, T. Jiang, G. Cheng, S. Wang, *Appl. Surf. Sci.* **257** (2011) 10126 (https://dx.doi.org/10.1016/j.apsusc.2011.06.161)
6. Y. Ryabenkova, N. Jadav, M. Conte, M. F. A. Hippler, N. Reeves-McLaren, P. D. Coates, P. Twigg, A. Paradkar, *Langmuir* **33** (2017) 2965 (https://dx.doi.org/10.1021/acs.langmuir.6b04510)
7. A. L. C. Maia, C. de Aguiar Ferreira, A. L. B. deBarros, A. T. M. e Silva, G. A. Ramaldes, A. da Silva Cunha Júnior, D. C. de Pádua Oliveira, C. Fernandes, D. C. F. Soares, *J. Drug Target.* **26** (2018) 592 (https://dx.doi.org/10.1080/1061186X.2017.1401078)
8. D. Loca, J. Locs, A. Dubnika, V. Zalite, L. Berzina-Cimdina, in H*ydroxyapatite (HAp) for Biomedical Applications*, M. Mucalo, Ed., 1st ed., Woodhead Publishing, Cambridge, 2015, pp.189–209 (Hardcover ISBN: 9781782420330)
9. Z. Yang, W. Xu, M. Ji, A. Xie, Y. Shen, M. Zhu, *Eur. J. Inorg. Chem.* (2017) 5621 (https://dx.doi.org/10.1002/ejic.201701081)

10. C. Bailly, *Drug Discov. Today* **24** (2019) 1930 (https://dx.doi.org/10.1016/j.drudis.2019.06.017)
11. L. Luo, F. Xu, H. Peng, Y. Luo, X. Tian, G. Battaglia, H. Zhang, Q. Gong, Z. Gu, K. Luo, *J. Control. Release* **318** (2020) 124 (https://dx.doi.org/10.1016/j.jconrel.2019.12.017)
12. R. T. Peterson, *Cell Chem. Biol.* **25** (2018) 1439 (https://dx.doi.org/10.1016/j.chembiol.2018.12.005)
13. N. H. Zuma, J. Aucamp, D. D. N'Da, *Eur. J. Pharm. Sci.* **140** (2019) 105092 (https://dx.doi.org/10.1016/j.ejps.2019.105092)
14. L. Chen, H. Zhu, S. Yang, B. Zhou, F. You, X. Yan, *Mater. Lett.* **143** (2015) 252 (https://dx.doi.org/10.1016/j.matlet.2014.12.118)
15. Ž. Radovanović, A. M. Kazuz, P. Vulić, L. Radovanović, Đ. Veljović, R. Petrović, Đ. Janaćković; in *Proceedings of 6th International Conference on Electrical, Electronic and Computing Engineering (Ic)ETRAN* (2019), Silver Lake, Serbia, *Proceedings_IcETRAN_ETRAN_2019*, ETRAN Society, Belgrade, Academic Mind, Belgrade, 2019, p. 676 (https://etran.rs/2019/Proceedings_IcETRAN_ETRAN_2019.pdf)
16. C. R. Groom, I. J. Bruno, M. P. Lightfoot, S. C. Ward, *Acta Crystallogr., B* **72** (2016) 171 (https://dx.doi.org/10.1107/S2052520616003954)
17. M. I. Toral, M. Paine, P. Leyton, P. Richter, *J. AOAC Int.* **87** (2004) 1323 (https://dx.doi.org/10.1093/jaoac/87.6.1323)
18. N. S. Sambudi, S. Cho, K. Cho, *RSC Adv.* **6** (2016) 43041 (https://dx.doi.org/10.1039/C6RA03147A)
19. T. Bera, A. N. Vivek, S. K. Saraf, P. Ramachandrarao, *Biomed. Mat.* **3** (2008) 025001 (https://dx.doi.org/10.1088/1748-6041/3/2/025001)
20. M. Ponjavić, M. S. Nikolić, J. Nikodinović-Runić, T. Ilić-Tomić, J. Djonlagić, *Int. J. Polym. Mater.* **68** (2019) 308 (https://dx.doi.org/10.1080/00914037.2018.1445631).